Iranian Journal of Numerical Analysis and Optimization
Vol. ??, No. ??, ??, pp ??
https://doi.org/??
https://ijnao.um.ac.ir/

Research Article

Traveling-wave patterns and bifurcation dynamics in a spatial predator-prey model

S. Hussain* and M. Sen

Abstract

We study a diffusive predator-prey model with nonlinear predator-prey interactions and prey dispersal. Using bifurcation analysis combined with numerical simulations, we reveal a rich variety of dynamical behaviors, including the stability of steady states, wave fronts, wave pulses, periodic and multi-periodic wave trains, and chaotic spatiotemporal patterns. The results show that diffusion and interaction strength play a critical role in shaping the traveling-wave dynamics through saddle-node, Hopf, and period-doubling bifurcations. In particular, increasing diffusion can destabilize steady states and induce oscillatory dynamics, ultimately leading to chaotic population fluctuations. These findings provide ecological insight into how spatial dispersal and nonlinear interactions shape complex population patterns in predator-prey systems.

AMS subject classifications (2020): Primary 37N25; Secondary 92-08, 92D25.

Keywords: Predator-Prey model; Traveling waves; Stability analysis; Bifurcation.

*Corresponding author

Received ??? ; revised ??? ; accepted ???

Saddam Hussain
Department of Mathematics and Computing Technology, NIT Patna, India 800005. e-mail: saddamh.phd20.ma@nitp.ac.in

Moitri Sen
Department of Mathematics and Computing Technology, NIT Patna, India 800005. e-mail: moitri300784@gmail.com

How to cite this article
Hussain, S. and Sen, M., Traveling-wave patterns and bifurcation dynamics in a spatial predator-prey model. *Iran. J. Numer. Anal. Optim.*, ??; ??(??): ??-??. ??

1 Introduction

The prey-predator model, commonly referred to as the Lotka–Volterra model, is a cornerstone of mathematical ecology and provides a fundamental framework for describing the dynamic interaction between two interdependent populations: prey, which constitute a food resource, and predators, which rely on prey for survival. This classical formulation has played a crucial role in advancing our understanding of population oscillations, species coexistence, and ecological balance. Over the years, the basic model has been extended in various directions to incorporate biological mechanisms observed in real ecosystems, thereby improving its ecological realism and predictive capacity. One important refinement of the classical predator-prey framework is the incorporation of cooperative hunting behavior among predators. In many natural systems, predators do not act independently but instead hunt in groups, thereby increasing capture efficiency and altering functional responses. Such cooperative strategies can significantly modify population dynamics by amplifying predation pressure and influencing stability properties of equilibria. The ecological relevance of cooperative hunting and its mathematical formulation were first systematically explored by Alves and Hilker [4], who demonstrated that predator cooperation can lead to qualitatively new dynamical behaviors not present in classical models.

While most early predator-prey models focused on temporal dynamics alone, spatial effects are now recognized as an essential component of ecological systems. Species movement, dispersal, and spatial heterogeneity strongly influence persistence, invasion, and pattern formation [25]. To capture these effects, predator-prey models are naturally extended to reaction-diffusion systems by incorporating diffusion terms that describe random movement in space. The inclusion of spatial dynamics is motivated by the seminal work of Turing on the chemical basis of morphogenesis [21], which demonstrated that diffusion, when coupled with nonlinear interactions, can destabilize homogeneous steady states and generate spatial patterns. From an ecological standpoint, reaction-diffusion predator-prey models provide a powerful framework for studying the combined effects of biological interactions and spatial dispersal [1]. In plankton communities, forest insect populations, and spatially structured food webs, population densities are rarely uniform across space. Instead, ecosystems often exhibit traveling invasion fronts, localized outbreaks, sustained oscillatory waves, and complex spatiotemporal patterns [8, 16]. Dispersal, commonly represented through diffusion, plays a dual role in such systems: it promotes persistence and spatial spread, yet can also destabilize homogeneous equilibria when coupled with nonlinear predation mechanisms, leading to oscillatory or even chaotic dynamics [13]. Consequently, the emergence of wave fronts, wave pulses, and wave trains in reaction-diffusion predator-prey models offers a mechanistic explanation for invasion processes, recurrent outbreaks, and cyclic population behavior observed in nature.

A particularly important mathematical tool for understanding these spatial phenomena is invariant manifold theory, which plays a central role in the analysis of traveling-wave solutions in reaction-diffusion systems. Traveling waves provide a mathematical description of spatial propagation processes occurring in diverse contexts, including population dynamics, nutrient transport, chemical reactions, and biological signal transmission [16, 15]. By introducing a moving coordinate frame, reaction-diffusion equations can be reduced to systems of ordinary differential equations, where traveling waves correspond to special trajectories in phase space. In this formulation, wave fronts, wave pulses, and wave trains arise as heteroclinic, homoclinic, and periodic orbits, respectively [13, 19, 24]. The existence and stability of these solutions are fundamentally governed by the geometry of invariant manifolds associated with equilibria and periodic orbits. Despite their conceptual importance, the rigorous construction of homoclinic and heteroclinic orbits remains a challenging problem, particularly in systems of dimension three or higher. Except for a few special cases, explicit analytical expressions for such connecting orbits are rarely available [8, 20]. As a result, a wide range of analytical and numerical techniques has been developed, including Poincaré maps, Lin's method, center manifold reductions, and numerical continuation, to establish the existence and continuation of global connections [9, 10, 14, 26]. In recent years, numerical bifurcation software such as `AUTO` [6] and `MATCONT` [5] has become indispensable for computing equilibria, periodic orbits, and their invariant manifolds with high accuracy, enabling systematic investigations of traveling waves in reaction-diffusion systems [18, 2, 11, 12].

Although traveling-wave solutions and diffusion-driven dynamics have been extensively investigated in predator-prey reaction-diffusion systems [7, 25, 22, 14], the combined effects of prey dispersal, a strong Allee effect, and cooperative hunting on traveling-wave dynamics remain largely unexplored. In contrast to [7, 14], where the emphasis is primarily on the existence of traveling waves and heteroclinic structures, the present work investigates how cooperative predation and prey diffusion interact to generate a rich bifurcation scenario involving wave fronts, pulse waves, periodic wave trains, multi-periodic oscillations, and chaotic traveling waves. Moreover, unlike [25] and [22], which focus on diffusion-driven instability and multiple wave solutions in more general reaction-diffusion settings, the present study reveals how hunting cooperation and prey dispersal jointly induce complex spatiotemporal behaviour through Hopf and period-doubling bifurcations. To the best of our knowledge, the emergence of chaotic traveling waves in a predator-prey system incorporating both cooperative hunting and Allee effects has not been previously reported.

Motivated by these developments, the objective of the present study is to investigate the existence and structure of traveling-wave solutions in a diffusive predator-prey model with nonlinear interaction terms. Building upon the predator-prey model proposed in [23], we focus on

the effects of prey dispersal on traveling-wave dynamics and the associated bifurcation structure. Using bifurcation theory, invariant manifold analysis, and numerical continuation techniques, we investigate how variations in diffusion and interaction parameters influence the qualitative behavior of traveling-wave solutions and lead to transitions between different dynamical regimes. The remainder of the paper is organized as follows. Section 2 introduces the reaction-diffusion model, analyzes the existence and stability of its equilibria, derives the traveling-wave equations, and investigates their phase-space structure. Section 3 employs numerical continuation methods to compute homoclinic and heteroclinic orbits and classify the resulting traveling-wave solutions. Finally, Section 4 discusses the ecological implications of our findings and summarizes the main conclusions of the study.

2 Diffusive model

We consider a prey-predator reaction-diffusion model obtained by introducing one-dimensional spatial diffusion only in the prey population, extending the nonspatial system (4) proposed in the paper [23]. The primary objective of the present work is to investigate the existence of traveling-wave solutions for the following system:

$$\begin{aligned} \frac{\partial N}{\partial t} &= N\Big(\sigma(1-N)(N-\beta) - (1+\alpha P)P\Big) + d\frac{\partial^2 N}{\partial x^2}, \\ \frac{\partial P}{\partial t} &= P\delta(1-P) + e(1+\alpha P)NP, \end{aligned} \tag{1}$$

where $N(x,t)$ and $P(x,t)$ denote the densities of the prey and predator populations at position x and time t, respectively. The parameter $d > 0$ represents the diffusion coefficient of the prey species, modeling its random movement in space, while the predator population is assumed to be immobile. This asymmetric diffusion assumption reflects situations in which prey species exhibit higher mobility than predators and has been widely adopted in ecological and epidemiological modeling frameworks.

The prey growth is governed by the Allee effect, represented by the term $\sigma(1-N)(N-\beta)$, where $\sigma > 0$ is the intrinsic growth rate of the prey and $\beta \in (-1,1)$ denotes the Allee threshold below, which the prey population experiences negative growth [3]. Predator consumption of prey follows a Holling type-I functional response, given by $(1+\alpha P)P$, where $\alpha \geq 0$ represents the strength of cooperative hunting among predators. It is assumed that predators hunt prey in groups, thereby enhancing their predation efficiency and increasing the prey capture rate. The predator population grows logistically in the absence of prey with intrinsic growth rate $\delta > 0$ and

carrying capacity normalized to unity. The term $e(1+\alpha P)NP$ represents the gain in predator biomass due to predation, where $e>0$ denotes the conversion efficiency of consumed prey into predator reproduction.

System (1) is inspired by the predator-prey framework introduced in [22], incorporating both the Allee effect in prey dynamics and a Holling type-I functional response. The inclusion of diffusion only in the prey equation allows the model to capture spatial propagation phenomena driven by prey dispersal, which plays a crucial role in the formation of traveling-wave solutions connecting biologically relevant equilibria. Such spatially structured dynamics are essential for understanding invasion processes, range expansion, and pattern formation in ecological systems.

2.1 Traveling-wave reduction

In order to study the traveling waves, we introduce the coordinate, $z=x-ct$, where $c>0$ denotes the wave speed, and seek solutions of the form $N(x,t)=U(z), \quad P(x,t)=V(z)$. Substitution into (1) yields

$$\begin{aligned} -cU' &= dU'' + U\Big(\sigma(1-U)(U-\beta)-(1+\alpha V)V\Big), \\ -cV' &= V\delta(1-V)+e(1+\alpha V)UV, \end{aligned} \tag{2}$$

where primes denote differentiation with respect to z. Introducing the auxiliary variable $W=U'$, system (2) can be rewritten as the following first-order autonomous system:

$$\begin{aligned} U' &= W, \\ W' &= \frac{1}{d}\Big(-cW-\sigma U(1-U)(U-\beta)+(1+\alpha V)UV\Big), \\ V' &= -\frac{1}{c}\Big(V\delta(1-V)+e(1+\alpha V)UV\Big). \end{aligned} \tag{3}$$

System (3) is three-dimensional, in contrast to the four-dimensional traveling-wave system obtained when both species diffuse. This reduction in dimension plays a crucial role in the qualitative analysis of wave solutions. Motivated by the biological context of (1), we confine our analysis of system (3) to the domain $\Omega=\{(U,W,V)\in\mathbb{R}^3 : U>0, V>0\}$. A traveling-wave solution of (1) is defined as any bounded solution of system (3) that lies entirely within the domain Ω. Such solutions represent wave profiles that move through space while maintaining their shape over time [15, 16, 8].

To obtain bounded solutions of system (3), we consider three principal classes of traveling waves: wave pulses, wave fronts, and wave trains. A wave pulse is associated with a homoclinic orbit of the traveling-wave system, in which a trajectory leaves an equilibrium point E_1 along its unstable manifold and returns to the same equilibrium along its stable manifold, so that the orbit lies in $W^u(E_1) \cap W^s(E_1)$. Such solutions display a pronounced excursion in the amplitudes of the state variables followed by convergence back to the resting state, and in the original reaction-diffusion system they correspond to localized pulses propagating through space while connecting a spatially homogeneous steady state to itself. A wave front, on the other hand, arises from a heteroclinic connection between two distinct equilibria, where the orbit departs from E_1 along $W^u(E_1)$ and approaches another equilibrium E_2 along its stable manifold $W^s(E_2)$, that is, it lies in $W^u(E_1) \cap W^s(E_2)$; this represents a traveling interface that connects two different spatially homogeneous steady states. Finally, wave trains correspond to periodic traveling-wave solutions of the reduced system, characterized by closed orbits in phase space. These solutions are spatially periodic and temporally steady in the moving frame, representing a continuous sequence of oscillations that propagate with constant speed without decay, and they play a key role in describing sustained rhythmic patterns in the underlying reaction-diffusion model [22].

2.2 Stability analysis

An equilibrium of (3) is given by $E = (U^*, 0, V^*)$, where (U^*, V^*) satisfies

$$\begin{aligned} U^*\Big(\sigma(1-U^*)(U^*-\beta) - (1+\alpha V^*)V^*\Big) &= 0, \\ V^*\Big(\delta(1-V^*) + e(1+\alpha V^*)U^*\Big) &= 0. \end{aligned} \tag{4}$$

From (4), we identify the following classes of equilibria.

(i) Trivial equilibrium.

$$E_0 = (0, 0, 0).$$

(ii) Boundary equilibria.

$$E_\beta = (\beta, 0, 0), \qquad E_1 = (1, 0, 0) \qquad E_2 = (0, 0, 1).$$

The equilibrium E_β, E_1 corresponds to extinction of the P-population and persistence of N and E_2 correspond to extinction of the N-population and persistence of P at its intrinsic steady states.

(iii) Coexistence equilibria. If $U^* > 0$ and $V^* > 0$, then (U^*, V^*) satisfies

$$\begin{aligned} \sigma(1-U^*)(U^*-\beta) &= (1+\alpha V^*)V^*, \\ \delta(1-V^*) + e(1+\alpha V^*)U^* &= 0. \end{aligned} \tag{5}$$

Due to the nonlinear coupling between U^* and V^*, explicit closed-form expressions for these quantities are generally difficult to obtain. Consequently, the coexistence equilibrium is characterized implicitly by system (5). For suitable parameter values, system (5) admits positive solutions, yielding the biologically relevant coexistence equilibrium

$$E_* = (U^*, 0, V^*).$$

2.2.1 Linearization and Jacobian matrix

The Jacobian matrix of (3) evaluated at an equilibrium $E = (U^*, 0, V^*)$ is given by

$$J(E) = \begin{pmatrix} 0 & 1 & 0 \\ -a_{11} & -\frac{c}{d} & -a_{13} \\ -a_{31} & 0 & -a_{33} \end{pmatrix},$$

where

$$\begin{aligned} a_{11} &= \frac{1}{d}\Big(\sigma(-3{U^*}^2 + 2(1+\beta)U^* - \beta) - (1+\alpha V^*)V^*\Big), \\ a_{13} &= -\frac{1}{d}\Big(1+2\alpha V^*\Big)U^*, \\ a_{31} &= \frac{e}{c}\Big(1+\alpha V^*\Big)V^*, \\ a_{33} &= \frac{1}{c}\Big(\delta(1-2V^*) + e(1+2\alpha V)U^*\Big). \end{aligned}$$

2.2.2 Characteristic equation

The characteristic polynomial of $J(E)$ takes the form

$$\lambda^3 + \left(\frac{c}{d} + a_{33}\right)\lambda^2 + \left(a_{11} + \frac{c}{d}a_{33}\right)\lambda + (a_{11}a_{33} - a_{13}a_{31}) = 0. \tag{6}$$

The signs of the coefficients in (6) determine the local stability properties of the equilibrium [17].

2.2.3 Stability of boundary equilibria

Lemma 1. The equilibrium point E_0 is a stable equilibrium whenever $-1 < \beta < 0$ with $dim^s(E_0) = 3$ and saddle whenever $0 < \beta < 1$ with $dim^s(E_0) = 2$, $dim^u(E_0) = 1$.

Proof. At E_0, the Jacobian reduces to

$$J(E_0) = \begin{pmatrix} 0 & 1 & 0 \\ \frac{\sigma\beta}{d} & -\frac{c}{d} & 0 \\ 0 & 0 & -\frac{\delta}{c} \end{pmatrix}.$$

The corresponding eigenvalues are

$$\lambda_{1,2} = \frac{-c \pm \sqrt{c^2 + 4\sigma\beta}}{2d}, \qquad \lambda_3 = -\frac{\delta}{c} < 0.$$

Hence, E_0 is a stable equilibrium whenever $-1 < \beta < 0$ on a three dimensional manifold and saddle whenever $0 < \beta < 1$ in two dimensional stable and one dimensional unstable manifold. □

Lemma 2. The equilibrium point E_β exist for $0 < \beta < 1$ and is a saddle with $dim^s(E_\beta) = 2$, $dim^u(E_\beta) = 1$

Proof. The Jacobian matrix at E_β is therefore

$$J(E_\beta) = \begin{pmatrix} 0 & 1 & 0 \\ -\frac{\sigma\beta(1-\beta)}{d} & -\frac{c}{d} & \frac{\beta}{d} \\ 0 & 0 & -\frac{\delta+e\beta}{c} \end{pmatrix}.$$

The eigenvalues satisfy

$$\lambda_{1,2} = \frac{-c \pm \sqrt{c^2 + 4\sigma\beta(1-\beta)}}{2d}, \qquad \lambda_3 = -\frac{\delta + e\beta}{c} < 0.$$

Thus, equilibrium E_β is a saddle point with a one-dimensional unstable manifold and a two-dimensional stable manifold. □

Lemma 3. The equilibrium point E_1 is a saddle equilibrium with $dim^s(E_1) = 2$, $dim^u(E_1) = 1$.

Proof. The Jacobian matrix at E_1 is

$$J(E_1) = \begin{pmatrix} 0 & 1 & 0 \\ \frac{\sigma(1-\beta)}{d} & -\frac{c}{d} & \frac{1}{d} \\ 0 & 0 & -\frac{\delta+e}{c} \end{pmatrix}.$$

The eigenvalues are

$$\lambda_{1,2} = \frac{-c \pm \sqrt{c^2 + 4\sigma(1-\beta)}}{2d}, \qquad \lambda_3 = -\frac{\delta+e}{c} < 0.$$

Hence, E_1 is also a saddle equilibrium with a two-dimensional stable manifold and a one-dimensional unstable manifold. □

Lemma 4. The equilibrium point E_2 is also a saddle equilibrium with $dim^s(E_2) = 1$, $dim^u(E_2) = 2$.

Proof. The Jacobian matrix at E_2 is given by

$$J(E_2) = \begin{pmatrix} 0 & 1 & 0 \\ \frac{\sigma\beta+1+\alpha}{d} & -\frac{c}{d} & 0 \\ -\frac{e(1+\alpha)}{c} & 0 & \frac{\delta}{c} \end{pmatrix}.$$

The characteristic polynomial of $J(E_2)$ is

$$(\lambda - \tfrac{\delta}{c})\left(d\lambda^2 + c\lambda - (\sigma\beta + 1 + \alpha)\right) = 0.$$

Hence, the eigenvalues are

$$\lambda_{1,2} = \frac{-c \pm \sqrt{c^2 + 4\big(\sigma\beta + 1 + \alpha\big)}}{2}, \qquad \lambda_3 = \frac{\delta}{c} > 0.$$

Since $\lambda_3 > 0$ and the quadratic term admits one positive and one negative root, equilibrium E_2 possesses a two-dimensional unstable manifold and a one-dimensional stable manifold. Therefore, E_2 is a saddle equilibrium of index two. □

2.2.4 Stability of coexistence equilibrium

If a coexistence equilibrium $E_* = (U^*, 0, V^*)$ exists, its local stability is determined by the eigenvalues of the Jacobian matrix evaluated at E_*. The corresponding characteristic equation is

$$\lambda^3 + \Big(\frac{c}{d} + b_{33}\Big)\,\lambda^2 + \frac{1}{d}\Big(b_{11} + cb_{33}\Big)\lambda + \frac{1}{d}\Big(b_{11}b_{33} - b_{13}b_{31}\Big) = 0, \tag{7}$$

where

$$\begin{aligned} b_{11} &= \sigma U^*(-2U^* + \beta + 1), \qquad & b_{13} &= -(1 + 2\alpha V^*)U^*, \\ b_{31} &= \tfrac{e}{c}\Big(1 + \alpha V^*\Big)V^*, \qquad & b_{33} &= \tfrac{1}{c}\Big(-\delta + e\alpha U^*\Big)V^*. \end{aligned}$$

By the Routh–Hurwitz criterion for cubic polynomials, the equilibrium E_* is locally asymptotically stable if and only if

$$\frac{c}{d} + b_{33} > 0, \qquad b_{11} + cb_{33} > 0, \qquad b_{11}b_{33} - b_{13}b_{31} > 0,$$

and

$$\Big(\frac{c}{d} + b_{33}\Big)\,(b_{11} + cb_{33}) > (b_{11}b_{33} - b_{13}b_{31})\,.$$

Although the stability conditions can be stated in terms of the coefficients of the characteristic polynomial, these coefficients depend nonlinearly on the model parameters and the equilibrium values U^* and V^*. Consequently, determining explicit parameter regions that guarantee stability or instability is analytically cumbersome. To gain further insight into the dynamics of the system and to investigate the influence of key parameters on the stability of the coexistence equilibrium E_*, we therefore complement the analytical results with numerical simulations. The numerical investigations presented in the next section illustrate the local behavior of solutions near E_* and identify parameter regimes associated with stable and unstable dynamics.

2.2.5 Hopf bifurcation analysis

The occurrence of Hopf bifurcation at the equilibrium point $E_* = (U^*, 0, V^*)$ is determined by the characteristic equation (7). According to the Hopf bifurcation theorem, a Hopf bifurcation occurs when a pair of complex conjugate eigenvalues of the Jacobian matrix $J(E_*)$ crosses the imaginary axis as a system parameter varies, while the remaining eigenvalue has a nonzero real part.

Let d be chosen as the bifurcation parameter. For (7) to admit a pair of purely imaginary roots $\lambda = \pm i\omega$ ($\omega > 0$), the following necessary conditions must be satisfied:

$$\frac{c}{d} + b_{33} > 0, \tag{8}$$

$$b_{13}b_{31} - b_{11}b_{33} > 0, \tag{9}$$

and the Hopf-bifurcation threshold is obtained by

$$d_H = -\frac{c(b_{11} + cb_{33})}{b_{13}b_{31} + cb_{33}^2}, \tag{10}$$

where

$$\omega^2 = \frac{1}{d}\Big(b_{11} + cb_{33}\Big). \tag{11}$$

In addition, the transversality condition must hold, namely,

$$\frac{d}{dd}\Re(\lambda(d))\Big|_{d=d_H} \neq 0. \tag{12}$$

This condition ensures that the eigenvalues cross the imaginary axis with nonzero speed as the bifurcation parameter d passes through the critical value d_H.

When all the above conditions are satisfied, the equilibrium point $E_* = (U^*, 0, V^*)$ undergoes a Hopf bifurcation at $d = d_H$. As a consequence, a family of small-amplitude periodic solutions emerges from E, leading to sustained oscillations in the population densities. These temporal oscillations play a crucial role in the formation of wave trains in the corresponding reaction-diffusion system, as will be demonstrated in the subsequent sections.

3 Numerical simulation

In this section, the traveling-wave system (3) was solved numerically using the classical fourth-order Runge–Kutta (RK4) method. Since traveling-wave solutions are defined on the unbounded domain $z \in (-\infty, \infty)$, the computational domain was truncated to the finite interval $[-L, L]$ with $L = 250$. Unless otherwise stated, the numerical simulations were performed using a uniform step size $h = 0.001$.

The numerical integration was initiated at $z = -L$ using initial data chosen in a sufficiently small neighborhood of the equilibrium state from which the traveling orbit originates. The solution was then integrated forward up to $z = L$. Since a fixed-step RK4 scheme was employed, no adaptive numerical tolerance parameter was required.

To verify the accuracy and robustness of the numerical computations, convergence tests were performed using different step sizes and computational domains. The resulting traveling-wave

profiles exhibited no significant qualitative or quantitative differences, confirming that the reported numerical solutions are independent of the discretization parameters and domain truncation. The parameter values were fixed according to the ecological model proposed in [23] and are summarized in Table 1.

Table 1: Parameter values used in numerical simulations.

s	β	e	δ	c
8	-0.108	0.17	0.2298	0.6

For these fixed parameters, numerical continuation and bifurcation analysis were carried out using the software package MATCONT. The primary objective of this study is to examine how variations in the hunting cooperation parameter α and the diffusion coefficient d influence the qualitative dynamics of the traveling-wave system (3). In particular, we investigate the stability of equilibria and the associated bifurcation structure, including saddle-node, Hopf, and period-doubling bifurcations.

The resulting bifurcation diagrams reveal transitions between different traveling-wave behaviors, including wave fronts, wave pulses, periodic and multi-periodic wave trains, and chaotic traveling patterns, highlighting the important roles of hunting cooperation and prey diffusion in shaping the spatiotemporal dynamics of the predator-prey system.

3.1 Bifurcation

For the chosen set of parameters, the boundary equilibrium points E_0, E_1, and E_2, together with the interior equilibrium E^*, coexist. Numerical bifurcation analysis reveals the occurrence of a saddle-node bifurcation at $\alpha = \alpha_{ZH}$, where the number of interior equilibrium points changes from two to zero as the parameter α is varied from left to right in Figure 1(a). In the parameter region where two interior equilibria exist, they are denoted by E_1^* and E_2^*. The blue curve in Figure 1(a) represents the Hopf bifurcation curve associated with the equilibrium E_1^*. Below this curve, E_1^* is locally asymptotically stable, whereas it loses stability upon crossing the curve, giving rise to periodic oscillations. In the unstable region of E_1^*, a period-doubling bifurcation occurs, indicated by the magenta curve. Inside the resulting period-doubling loop, solutions with higher-order periodicity, including 2-periodic, 4-periodic, and chaotic dynamics, are observed, indicating a classical route to chaos. The red curve corresponds to the Hopf bifurcation associated with the equilibrium E_2^*. Below this curve, E_2^* is a saddle-focus with one positive real eigenvalue and the

remaining eigenvalues having negative real parts, whereas above the curve, the real parts of the complex conjugate eigenvalues become positive, leading to oscillatory instability.

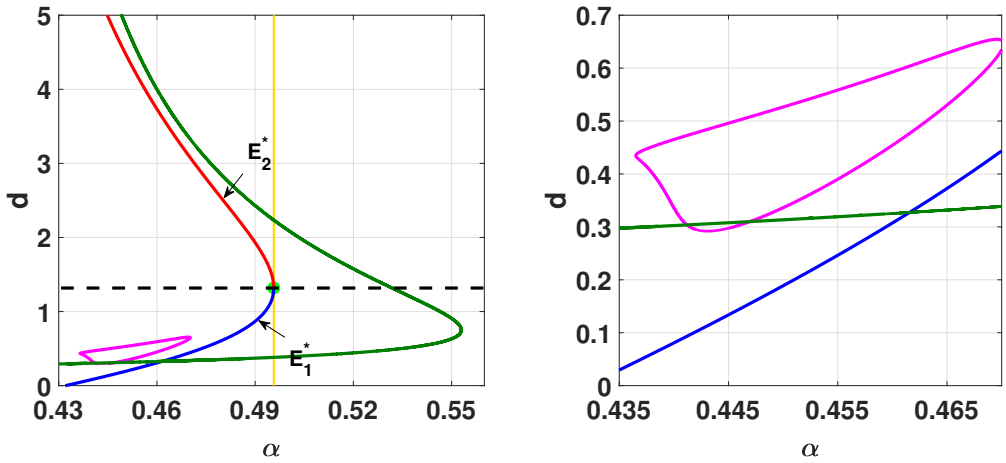

(a) (b)

Figure 1: (a) Two-dimensional bifurcation diagram with respect to α and d. The yellow vertical line shows the saddle-node bifurcation curve, the red curve shows the Hopf bifurcation curve for the equilibrium E_2^*, the blue curve shows the Hopf-bifurcation for the equilibrium E_1^* and the magenta curve represents the period-doubling bifurcation curve.The green curve represents the homoclinic bifurcation curve. The green dot represents the zero-Hopf point. (b) The zoomed version of Figure 1(a).

Figure 2 presents the one-dimensional bifurcation diagrams obtained by plotting the local maxima and minima of the prey and predator densities with respect to the diffusion coefficient d, while keeping the parameter $\alpha = 0.44$ fixed. For small values of d, both species converge to a constant equilibrium state, which is reflected in the diagram by a single branch for each variable. This indicates that the equilibrium is locally asymptotically stable in this parameter regime. As d increases and crosses a critical threshold, the equilibrium loses stability through a Hopf bifurcation, leading to the emergence of sustained oscillations. Beyond this point, the bifurcation diagrams split into two distinct branches corresponding to the maximum and minimum values attained by the prey and predator populations, thereby signaling periodic oscillatory dynamics.

With a further increase in the diffusion coefficient d, the system undergoes a sequence of secondary bifurcations. The appearance of multiple discrete branches in the bifurcation diagrams corresponds to period-doubling bifurcations, where oscillations with twice the original period are generated. This cascade continues as d increases, resulting in increasingly complex oscillatory patterns, including 2-periodic, 4-periodic, and higher-order periodic solutions. Eventually, the accumulation of these bifurcations gives rise to chaotic dynamics, which are manifested in the diagrams as densely populated bands of maxima and minima. This behavior is observed consis-

tently for both prey and predator species, demonstrating that diffusion plays a crucial role in destabilizing the equilibrium and driving the system through a transition from steady states to periodic oscillations and ultimately to chaotic spatiotemporal dynamics.

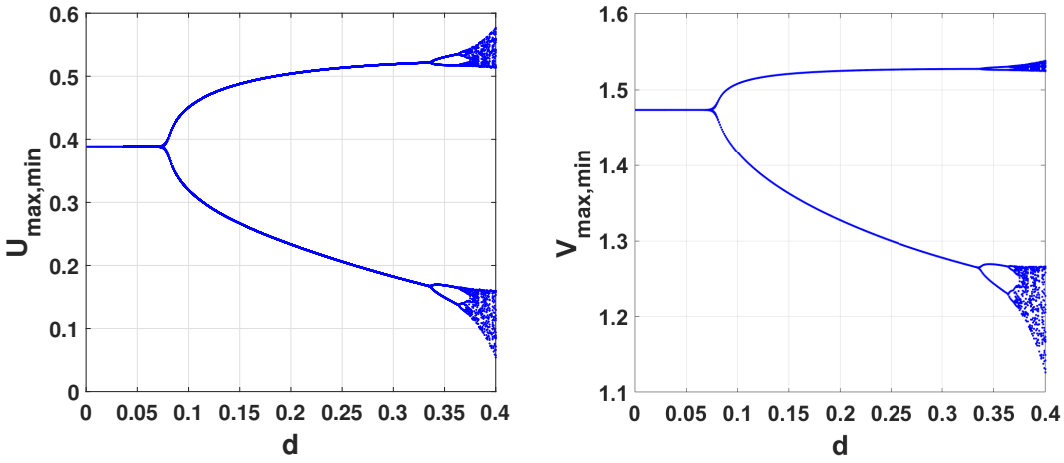

(a) (b)

Figure 2: One dimensional bifurcation diagram with respect to the diffusion coefficient d for fixed $\alpha = 0.44$, (a) prey species and (b) predator species.

To determine the nature of the Hopf bifurcation, the first Lyapunov coefficient was computed numerically using MATCONT. For the parameter value $\alpha = 0.44$, the Hopf bifurcation occurs at

$$d_H = 0.080745985,$$

and the corresponding first Lyapunov coefficient is

$$l_1 = -5.39211921 < 0.$$

Therefore, the Hopf bifurcation is supercritical, and a branch of stable periodic solutions emerges from the coexistence equilibrium as the diffusion coefficient d passes through the critical value d_H. This observation is consistent with the numerical bifurcation diagrams presented in the subsequent section.

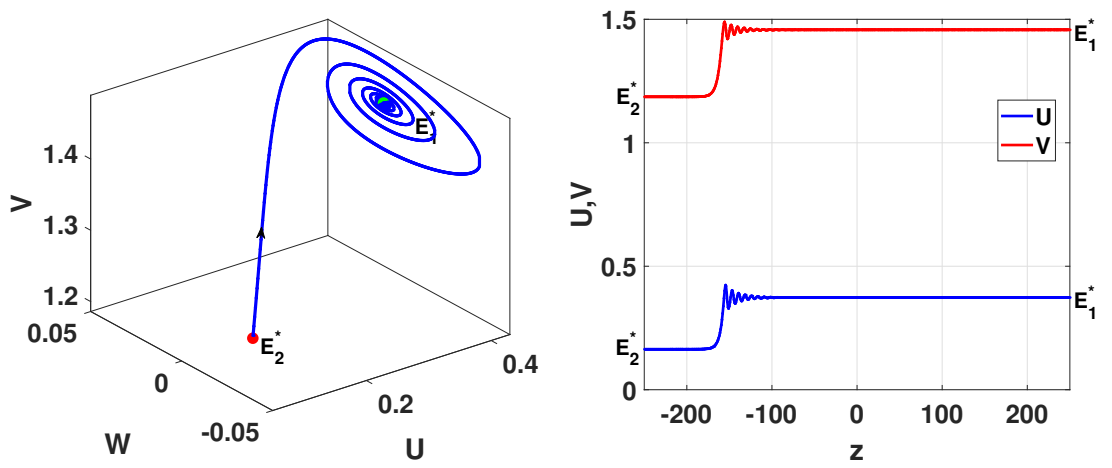

(a) (b)

Figure 3: (a) Phase portrait of the traveling-wave system showing convergence to a stable spiral equilibrium. (b) Corresponding spatial profiles of the prey (U) and predator (V) populations. Parameter values are $\alpha = 0.45$ and $d = 0.1$.

3.2 Phase portrait

To validate the bifurcation diagram shown in Figure 1, we present the corresponding phase portrait and spatial profiles of the prey and predator populations. For parameter values chosen from the regime in which the equilibrium E_1^* is stable, namely $\alpha = 0.45$ and $d = 0.1$, the traveling-wave system admits a heteroclinic connection between two distinct equilibria. As shown in Figure 3, the phase portrait indicates that the trajectory originates in the neighborhood of the equilibrium E_2^* and departs along its unstable manifold. After a transient evolution, the orbit approaches and eventually settles at the equilibrium E_1^* along its stable manifold, confirming the existence of a heteroclinic orbit lying in the intersection $W^u(E_2^*) \cap W^s(E_1^*)$. The corresponding spatial profiles of the state variables, depicted in Figure 3(b), clearly illustrate a transition from the state associated with E_2^* to that of E_1^*, with small oscillations observed as the solution converges to the final steady state. In the context of the original reaction-diffusion system, this heteroclinic connection represents a wave front, describing a traveling interface that propagates with constant speed and connects two distinct spatially homogeneous equilibrium states.

For parameter values taken from the regime in which the equilibrium E_1^* loses stability through a Hopf bifurcation, specifically $\alpha = 0.45$ and $d = 0.25$, the traveling-wave system exhibits a heteroclinic-type connection from the equilibrium E_2^* to a periodic orbit generated at E_1^*. As illustrated by the phase portrait in Figure 4(a), the trajectory departs from the equilibrium E_2^*

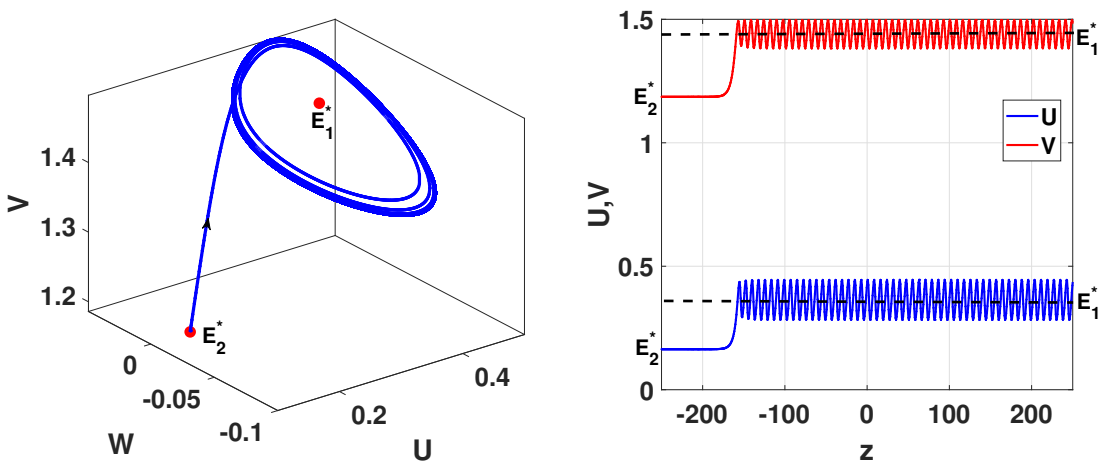

(a) (b)

Figure 4: (a) Phase portrait of the traveling-wave system showing convergence to a stable limit cycle. (b) Corresponding spatial profiles of the prey (U) and predator (V) populations. Parameter values are $\alpha = 0.45$ and $d = 0.25$.

along its unstable manifold and, instead of converging to a steady equilibrium, it is attracted to a stable limit cycle that emerges due to the Hopf bifurcation at E_1^*. This indicates that the orbit lies in the intersection of the unstable manifold of E_2^* and the stable manifold of the periodic orbit associated with E_1^*. The corresponding spatial profiles of the state variables, shown in Figure 4(b), display a transition from the homogeneous state corresponding to E_2^* to sustained oscillations with constant amplitude as the traveling coordinate z increases. In the original reaction-diffusion system, this behavior corresponds to a wave train solution, characterized by spatially periodic oscillations that propagate with a constant wave speed, representing a traveling pattern that connects a steady state to a stable periodic wave.

Continuing from the previous wave-train scenario, when the parameters are chosen from the region inside the magenta loop in Figure 1, specifically $\alpha = 0.45$ and $d = 0.4$, the traveling-wave system exhibits a further qualitative change in its dynamics. In this case, the equilibrium E_1^* gives rise to a stable 2-periodic orbit, as illustrated by the phase portrait in Figure 5(a). The corresponding spatial profiles of the prey and predator variables, shown in Figure 5(b), display sustained oscillations with two distinct peaks per period along the traveling coordinate. In the original reaction-diffusion framework, this behavior corresponds to a 2-periodic wave train, representing a more complex traveling pattern that emerges as a continuation of the wave-train solutions observed for smaller values of d.

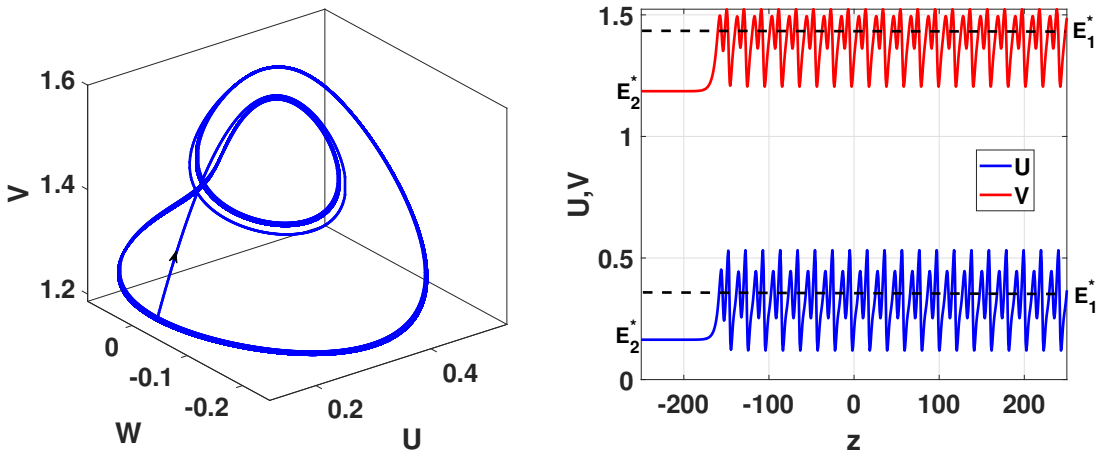

(a) (b)

Figure 5: (a) Phase portrait of the traveling-wave system showing 2-period oscillations. (b) Corresponding spatial profiles of the prey (U) and predator (V) populations. Parameter values are $\alpha = 0.45$ and $d = 0.4$.

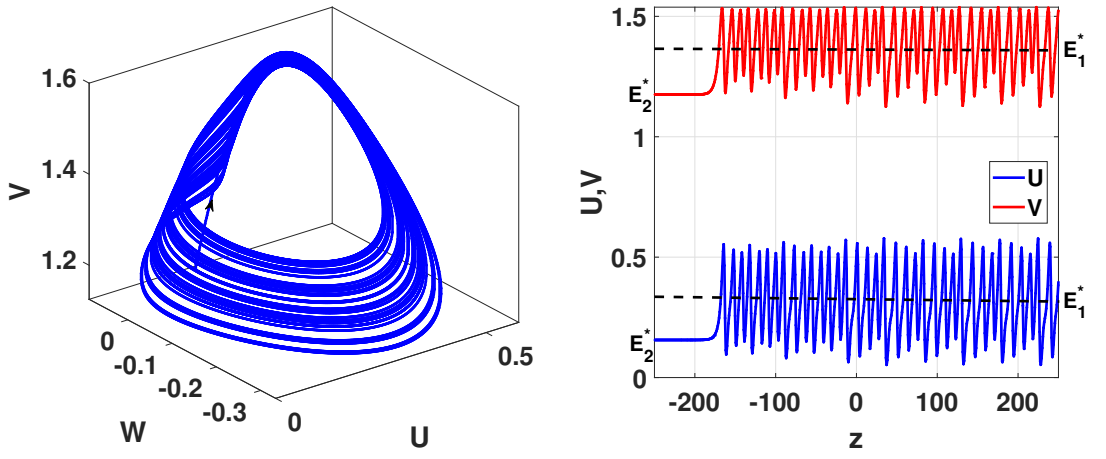

(a) (b)

Figure 6: (a) Phase portrait of the traveling-wave system showing chaotic behavior. (b) Corresponding spatial profiles of the prey (U) and predator (V) populations. Parameter values are $\alpha = 0.44$ and $d = 0.4$.

As a further continuation of the wave-train dynamics discussed above, a more complex behavior is observed when the parameters are chosen as $\alpha = 0.44$ and $d = 0.4$. In this regime, the equilibrium E_2^* no longer supports periodic motion but instead gives rise to chaotic dynamics, as evidenced by the irregular trajectory in the phase portrait shown in Figure 6(a). The corresponding spatial profiles of the prey and predator variables, depicted in Figure 6(b), exhibit aperiodic oscillations with varying amplitudes along the traveling coordinate. In the original reaction-diffusion system, this behavior corresponds to a chaotic wave train, representing a breakdown of regular periodic wave trains and highlighting a transition from periodic to chaotic traveling patterns as parameters vary.

To further verify the presence of chaos, the largest Lyapunov exponent was computed using the standard Benettin algorithm. Let $\delta U(0)$ denote an infinitesimal perturbation of the trajectory $U(z)$. The largest Lyapunov exponent is defined by

$$\lambda_{\max} = \lim_{z\to\infty} \frac{1}{z} \ln \left| \frac{\delta U(z)}{\delta U(0)} \right|. \tag{13}$$

A positive value of $\lambda_{\max}$ indicates exponential divergence of nearby trajectories and therefore provides a quantitative signature of chaotic dynamics, whereas $\lambda_{\max} < 0$ corresponds to stable dynamics. Figure 7 depicts the variation of the largest Lyapunov exponent with respect to the diffusion coefficient d. It can be observed that $\lambda_{\max}$ remains negative for small values of d, indicating stable dynamics. As d increases, $\lambda_{\max}$ approaches zero, corresponding to the onset of oscillatory behavior through Hopf bifurcation. Furthermore, for the parameter value used in Figure 6, the largest Lyapunov exponent is found to be

$$\lambda_{\max} = 0.0243034466 > 0,$$

which confirms that the irregular traveling-wave pattern shown in Figure 6 is indeed chaotic. Thus, Figure 7 provides quantitative evidence supporting the chaotic traveling-wave dynamics observed in Figure 6.

Figure 8 illustrates the emergence of a pulse-type traveling wave for the parameter values $\alpha = 0.439$ and $d = 0.30151634$ taken from the bifurcation diagram in Figure 1. Panel (a) shows the phase portrait of the traveling-wave system in the (U, V)-plane. The trajectory originates from the saddle equilibrium point E_2, makes a large excursion in phase space, and eventually returns to the same equilibrium. This closed connecting orbit represents a homoclinic orbit to E_2, indicating the occurrence of a homoclinic bifurcation. Such a global bifurcation arises when the limit cycle generated through a Hopf bifurcation grows in amplitude and collides with the saddle equilibrium as the diffusion parameter d is increased.

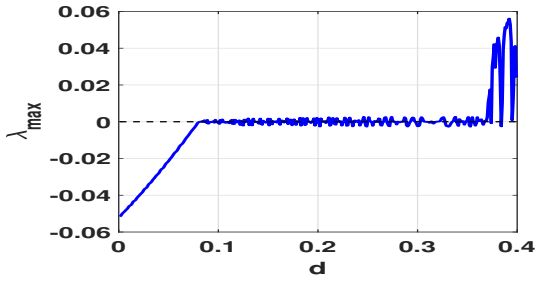

Figure 7: Variation of the largest Lyapunov exponent $\lambda_{\max}$ with respect to the diffusion coefficient d for fixed $\alpha = 0.44$.

The corresponding spatial profiles of the prey and predator densities are displayed in panel (b), respectively. The prey density $U(z)$ exhibits a sharp localized peak followed by a rapid decay to the equilibrium level, while the predator density $V(z)$ shows a pronounced overshoot before relaxing back to its steady state. These localized structures confirm the formation of a traveling pulse, characterized by a large deviation from the background equilibrium over a finite spatial region and convergence to the same equilibrium state as $z \to \pm\infty$.

Ecologically, the pulse wave corresponds to a transient but intense outbreak of prey followed by a delayed predator response, after which both populations return to their background densities. Such pulse-like invasion events are commonly observed in ecological systems where dispersal and strong predator-prey interactions interact to produce localized population bursts.

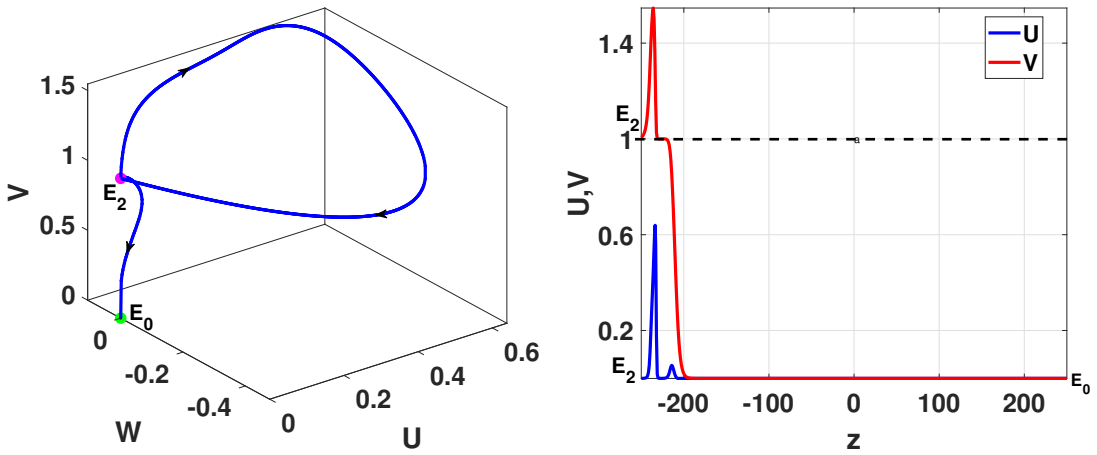

(a) (b)

Figure 8: (a) Phase portrait of the traveling-wave system showing a pulse wave. (b) Corresponding spatial profiles of the prey (U) and predator (V) populations. Parameter values are $\alpha = 0.439$ and $d = 0.30151634$.

4 Discussion and Conclusion

In this work, we investigated a diffusive predator-prey model governed by the system (1) with particular emphasis on the role of diffusion and nonlinear predator-prey interactions in shaping spatiotemporal population dynamics. Through a combination of analytical bifurcation analysis and extensive numerical simulations, we revealed a rich spectrum of dynamical behaviors, including steady states, wave fronts, wave pulses, periodic wave trains, multi-periodic oscillations, and chaotic traveling patterns.

The bifurcation analysis demonstrated that the system admits multiple boundary and interior equilibria, whose existence and stability strongly depend on the interaction parameter α and the diffusion coefficient d. A saddle-node bifurcation was identified at a critical value $\alpha = \alpha_{ZH}$, where the number of interior equilibria changes, marking a fundamental reorganization of the system's ecological structure. Hopf bifurcation curves associated with the interior equilibria delineate parameter regions where uniform population distributions lose stability and give rise to oscillatory dynamics. In particular, one interior equilibrium undergoes a Hopf bifurcation leading to stable periodic oscillations, while further parameter variation results in a cascade of period-doubling bifurcations culminating in chaotic behavior.

The one-dimensional bifurcation diagrams obtained by plotting the maxima and minima of prey and predator densities with respect to the diffusion coefficient clearly illustrate how increasing diffusion destabilizes spatially homogeneous equilibria. For small diffusion rates, both species settle at stable equilibrium densities, corresponding to ecological coexistence. As diffusion increases beyond a critical threshold, oscillatory dynamics emerge, followed by multi-periodic and chaotic fluctuations. This indicates that diffusion, often interpreted ecologically as dispersal or movement of species, can act as a destabilizing mechanism that promotes complex population cycles rather than spatial homogenization.

The traveling-wave analysis further revealed the ecological mechanisms underlying spatial pattern formation. Homoclinic orbits correspond to wave pulses, representing localized population outbreaks that propagate through space and eventually decay, while heteroclinic orbits give rise to wave fronts connecting distinct ecological states, such as transitions from low-density to high-density population regimes. Moreover, periodic and multi-periodic wave trains were shown to arise through Hopf and period-doubling bifurcations, representing sustained spatial oscillations in prey and predator densities. The emergence of chaotic wave trains highlights the possibility of irregular, unpredictable population patterns driven purely by intrinsic nonlinear interactions and dispersal.

From an ecological perspective, the cooperation parameter α quantifies the intensity of hunting cooperation among predators. Larger values of α correspond to stronger cooperative effects,

whereby predators benefit from coordinated hunting strategies, information sharing, or collective attacks, leading to enhanced predation efficiency. Such cooperative behavior has been documented in several social predator populations, including wolves, lions, African wild dogs, and dolphins. Consequently, variations in α may significantly influence species coexistence, population persistence, and the stability of ecological communities.

The results further demonstrate that prey dispersal can act as an important ecological mechanism capable of generating complex spatiotemporal dynamics. Although diffusion is commonly associated with spatial mixing and homogenization, the present analysis shows that increasing the prey diffusion coefficient can destabilize stable coexistence states and induce periodic, multi-periodic, and chaotic oscillations. Ecologically, diffusion-induced chaos implies that small changes in the spatial distribution of prey may lead to large and unpredictable fluctuations in both prey and predator populations, thereby affecting ecosystem stability and the predictability of population outbreaks.

The traveling-wave solutions obtained in this study also possess clear ecological interpretations. Wave fronts correspond to invasion processes in which one ecological state gradually replaces another as populations spread through space, whereas pulse waves represent localized population outbreaks that propagate through a finite spatial region before returning to the background equilibrium state. Similar pulse-like propagation phenomena have been reported in biological invasions, forest insect outbreaks, locust population expansions, and epidemic spreading processes. Furthermore, the chaotic traveling waves observed in the present model describe irregular invasion fronts whose amplitudes and spatial structures vary unpredictably in space. Comparable spatiotemporal complexity has been reported in plankton ecosystems, vegetation dynamics in semi-arid environments, and predator-prey communities exhibiting strong nonlinear interactions.

Overall, the present study highlights the important roles of prey dispersal and cooperative hunting in shaping ecological dynamics. The interplay between diffusion, nonlinear interactions, and cooperative predation generates a rich variety of traveling-wave structures, ranging from wave fronts and pulse waves to periodic and chaotic wave trains. These findings provide valuable insight into the mechanisms responsible for spatial population patterns, invasion phenomena, recurrent outbreaks, and irregular spatiotemporal fluctuations observed in ecological systems.

Funding

This research received no external funding.

Conflicts of Interest

The authors declare that they have no conflicts of interest. All authors jointly worked on the results, read and approved the final manuscript, and declare that they have no competing interests.

References

[1] Aguirre, P., Flores, J.D. and González-Olivares, E. *Bifurcations and global dynamics in a predator–prey model with a strong Allee effect on the prey, and a ratio-dependent functional response*, Nonlinear Anal. Real World Appl. 16 (2014), 235–249.

[2] Aguirre, P., Krauskopf, B. and Osinga, H.M. *Global invariant manifolds near a Shilnikov homoclinic bifurcation*, J. Comput. Dyn. 1(1) (2014) 1–38.

[3] Allee, W.C. *Animal aggregations: A study in general sociology*, University of Chicago Press, Chicago, 1931.

[4] Alves, M.T. and Hilker, F.M. *Hunting cooperation and Allee effects in predators*, J. Theor. Biol. 419 (2017), 13–22.

[5] Dhooge, A., Govaerts, W., Kuznetsov, Y.A., Meijer, H.G.E. and Sautois, B. *New features of the software MatCont for bifurcation analysis of dynamical systems*, Math. Comput. Model. Dyn. Syst. 14(2) (2008), 147–175.

[6] Doedel, E.J., Champneys, A.R., Dercole, F., Fairgrieve, T.F., Kuznetsov, Y.A., Oldeman, B., Paffenroth, R.C., Sandstede, B., Wang, X.J. and Zhang, C.H. *AUTO-07P: Continuation and bifurcation software for ordinary differential equations*, Concordia University, 2007.

[7] Dunbar, S.R. *Traveling waves in diffusive predator–prey equations: periodic orbits and point-to-periodic heteroclinic orbits*, SIAM J. Appl. Math. 46(6) (1986), 1057–1078.

[8] Homburg, A.J. and Sandstede, B. *Homoclinic and heteroclinic bifurcations in vector fields*, in: Handbook of Dynamical Systems, Vol. 3, Elsevier, 2010, 379–524.

[9] Hsu, C.H., Yang, C.R., Yang, T.H. and Yang, T.S., *Existence of traveling wave solutions for diffusive predator–prey type systems*, J. Differ. Equ. 252(4) (2012), 3040–3075.

[10] Huang, J., Lu, G. and Ruan, S. *Existence of traveling wave solutions in a diffusive predator–prey model*, J. Math. Biol. 46(2) (2003), 132–152.

[11] Krauskopf, B. and Osinga, H.M. *Computing invariant manifolds via the continuation of orbit segments*, in: Numerical Continuation Methods for Dynamical Systems, Springer, 2007, 117–154.

[12] Krauskopf, B., Osinga, H.M., Doedel, E.J., Henderson, M.E., Guckenheimer, J., Vladimirsky, A., Dellnitz, M. and Junge, O. *A survey of methods for computing (un)stable manifolds of vector fields*, Int. J. Bifurc. Chaos, 15(3) (2005), 763–791.

[13] Li H. and Xiao, H. *Traveling wave solutions for diffusive predator–prey type systems with nonlinear density dependence*, Comput. Math. Appl. 74(10) (2017), 2221–2230.

[14] Manna, K., Pal, S. and Banerjee, M. *Analytical and numerical detection of traveling wave and wave-train solutions in a prey–predator model with weak Allee effect*, Nonlinear Dyn. 100(3) (2020), 2989–3006.

[15] Murray, J.D. *Mathematical biology*, Springer-Verlag, Berlin, 1989.

[16] Murray, J.D. *Spatial models and biomedical applications*, Mathematical Biology, Springer, 2003.

[17] Perko, L. *Differential equations and dynamical systems*, Vol. 7, Springer Science & Business Media, 2013.

[18] Sandstede, B. *Stability of N-fronts bifurcating from a twisted heteroclinic loop and an application to the FitzHugh–Nagumo equation*, SIAM J. Math. Anal., 29(1) (1998), 183–207.

[19] Sherratt, J.A. and Smith, M.J. *Periodic traveling waves in cyclic populations: field studies and reaction–diffusion models*, J. R. Soc. Interface. 5(22) (2008), 483–505.

[20] Takahashi, L.T., Maidana, N.A., Ferreira Jr, W.C., Pulino, P. and Yang, H.M. *Mathematical models for the Aedes aegypti dispersal dynamics: Traveling waves by wing and wind*, Bull. Math. Biol. 67(3) (2005), 509–528.

[21] Turing, A.M. *The chemical basis of morphogenesis*, Bull. Math. Biol. 52(1) (1990), 153–197.

[22] Villar-Sepúlveda, E., Aguirre, P. and Breña-Medina, V.F. *A case study of multiple wave solutions in a reaction-diffusion system using invariant manifolds and global bifurcations*, SIAM J. Appl. Dyn. Syst. 22(2) (2023), 918–950.

[23] Vishwakarma, K. and Sen, M. *Role of Allee effect in prey and hunting cooperation in a generalist predator*, Math. Comput. Simul. 190 (2021), 622–640.

[24] Wu, X., Luo, Y. and Hu, Y. *Traveling waves in a diffusive predator–prey model incorporating a prey refuge*, Abstract. Appl. Anal. 2014 (2014), Article ID 679131.

[25] Yadav, R., Sen, M. and Pal, S. *Impact of diffusion-driven instability on traveling wave solutions*, Phys. Rev. E. 111(2) (2025), 024202.

[26] Yamashita, W.M., Takahashi, L.T. and Chapiro, G. *Traveling wave solutions for the dispersive models describing population dynamics of Aedes aegypti*, Math. Comput. Simul. 146 (2018), 90–99.